# A simple model for the resonance shift of localized plasmons due to dielectric particle adhesion

**Tomasz J. Antosiewicz*, S. Peter Apell, Virginia Claudio, and Mikael Käll**

*Chalmers University of Technology, Department of Applied Physics,*
*SE-412 96 Göteborg, Sweden*

**tomasza@chalmers.se*

**Abstract:** Ultrasensitive detectors based on localized surface plasmon resonance refractive index sensing are capable of detecting very low numbers of molecules for biochemical analysis. It is well known that the sensitivity of such sensors crucially depend on the spatial distribution of the electromagnetic field around the metal surface. However, the precise connection between local field enhancement and resonance shift is seldom discussed. Using the quasistatic approximation, we developed a model that relates the sensitivity of a nanoplasmonic resonator to the local field in which the analyte is placed. The model, corroborated by finite-difference time-domain simulations, may be used to estimate the magnitude of the shift as a function of the properties of the sensed object – permittivity and volume – and its location on the surface of the resonator. It requires only a computation of the resonant field induced by the metal structure and is therefore suitable for numerical optimization of nanoplasmonic sensors.

**OCIS codes:** (240.6680) Surface plasmons, (240.6490) Surface-enhanced spectroscopy, (280.0280) Optical sensing and sensors

---

## References and links

1. P. Englebienne, "Use of colloidal gold surface plasmon resonance peak shift to infer affinity constants from the interactions between protein antigens and antibodies specific for single or miltiple epitopes," Analyst **123**, 1599–1603 (1998).
2. T. Okamoto, I. Yamaguchi, and T. Kobayashi, "Local plasmon sensor with gold colloid monolayers deposited upon glass substrates," Opt. Lett. **25**, 372–374 (2000).
3. M. D. Malinsky, K. L. Kelly, G. C. Schatz, and R. P. Van Duyne, "Chain length dependence and sensing capabilities of the localized surface plasmon resonance of silver nanoparticles chemically modified with alkanethiol self-assembled monolayers," J. Am. Chem. Soc. **123**, 1471–1482 (2001).
4. N. Nath and A. Chilkoti, "A colorimetric gold nanoparticle sensor to interrogate biomolecular interactions in real time on a surface," Anal. Chem. **74**, 504–509 (2002).
5. A. J. Haes and R. P. Van Duyne, "A nanoscale optical biosensor: Sensitivity and selectivity of an approach based on the localized surface plasmon resonance spectroscopy of triangular silver nanoparticles," J. Am. Chem. Soc. **124**, 10596–10604 (2002).
6. H. Xu and M. Käll, "Modeling the optical response of nanoparticle-based aurface plasmon resonance sensors," Sens. Actuators B Chem. **87**, 244–249 (2002).
7. J. N. Anker, W. P. Hall, O. Lyandres, N. C. Shah, J. Zhao, and R. P. Van Duyne, "Biosensing with plasmonic nanosensors," Nature Mat. **7**, 442–453 (2008).
8. J. Homola, *Surface plasmon resonance based sensors*, Springer Series on Chemical Sensors and Biosensors (Springer-Verlag, Berlin-Heidelberg-New York, 2006).

9. H. Xu, J. Aizpurua, M. Käll, and P. Apell, “Electromagnetic contributions to single-molecule sensitivity in surface-enhanced raman scattering,” Phys. Rev. E **62**, 4318–4324 (2000).
10. H. Xu, E. J. Bjerneld, M. Käll, and L. Börjesson, “Spectroscopy of single hemoglobin molecules by surface enhanced raman scattering,” Phys. Rev. Lett. **83**, 4357–4360 (1999).
11. L. Rodríguez-Lorenzo, R. A. Álvarez-Puebla, I. Pastoriza-Santos, S. Mazzucco, O. Stéphan, M. Kociak, L. M. Liz-Marzán, and F. J. G. de Abajo, “Zeptomol detection through controlled ultrasensitive surface-enhanced Raman scattering,” J. Am. Chem. Soc. **131**, 4616–4618 (2009).
12. T. Dadosh, J. Sperling, G. W. Bryant, R. Breslow, T. Shegai, M. Dyshel, G. Haran, and I. Bar-Joseph, “Plasmonic control of the shape of the raman spectrum of a single molecule in a silver nanoparticle dimer,” ACS Nano **3**, 1988–1994 (2009).
13. D.-K. Lim, K.-S. Jeon, H. M. Kim, J.-M. Nam, and Y. D. Suh, “Nanogap-engineerable Raman-active nanodumbbells for single-molecule detection,” Nature Mat. **9**, 60–67 (2010).
14. A. Unger, U. Rietzler, R. Berger, and M. Kreiter, “Sensitivity of crescent-shaped metal nanoparticles to attachment of dielectric colloids,” Nano Lett. **9**, 2311–2315 (2009).
15. T. Sannomiya, C. Hafner, and J. Voros, “In situ sensing of single binding events by localized surface plasmon resonance,” Nano Lett. **8**, 3450–2455 (2008).
16. T. Davis, D. Gómez, and K. Vernon, “Interaction of molecules with localized surface plasmons in metallic nanoparticles,” Phys. Rev. B **81**, 045423 (2010).
17. T. J. Davis, K. C. Vernon, and D. E. Gómez, “Designing plasmonic systems using optical coupling between nanoparticles,” Phys. Rev. B **79**, 155423 (2009).
18. F. Wang and Y. R. Shen, “General properties of local plasmons in metal nanostructures,” Phys. Rev. Lett. **97**, 206806 (2006).
19. P. Johnson and R. Christy, “Optical constants of the noble metals,” Phys. Rev. B **6**, 4370–4379 (1972).
20. O. Kedem, A. B. Tesler, A. Vaskevich, and I. Rubinstein, “Sensitivity and optimization of localized surface plasmon resonance transducers,” ACS Nano **5**, 748–760 (2011).
21. J. R. Zurita-Sánchez, “Quasi-static electromagnetic fields created by an electric dipole in the vicinity of a dielectric sphere: method of images,” Rev. Mex. Fis. **55**, 443–449 (2009).

## 1. Introduction

Plasmonics, that is the properties and applications of surface plasmons in metal structures, has become one of the most rapidly expanding fields in nanoscience and a cornersone of nanooptics. This development has become possible due to considerable progress in nanofabrication techniques and computational electromagnetics. However, the most important driver has been the potential for applications in areas such as the life sciences, photonics and solar energy research. Metal nanostructures exhibit localized surface plasmon resonances (LSPRs) determined primarily by their shape, size and material composition. But LSPRs are also utterly sensitive to the presence of nearby dielectric objects, and the optical response of such objects are in turn strongly affected by the localized electromagnetic field induced by the plasmon charge oscillation. These effects are the basis for one of the most exciting application opportunities in plasmonics, i.e. to use the localized plasmons to probe the presence of molecules that reside in the vicinity of the metal surface. This can be accomplished through amplification of the molecular vibrational fingerprint, like in surface-enhanced Raman scattering (SERS) and surface-enhanced infrared absorption (SEIRA), or by affecting molecular fluorescence properties. However, the most general approach is to monitor how the localized plasmon resonance itself changes in the presence of a molecule by measuring the color of the nanostructure [1-7]. This approach, which is essentially analogous to classical thin film surface plasmon resonance (SPR) refractive index sensing [8], is the focus of the present contribution.

The relation between optical response and the location of a molecular target relative to a plasmonic nanostructure is well established in the case of surface-enhanced spectroscopies. The amplitude of a SERS signal, for example, scales roughly as the fourth power of the local field-enhancement factor, which implies that “hot spots,” such as sharp tips or crevices between particles, may dominate completely [9]. Indeed, enhancement factors as high as ten orders-of-magnitude has been realized in single molecule SERS experiments [10-13]. But the position of an analyte molecule is also expected to affect the response of a LSPR refractive index sensor

[14, 15]. This effect was recently analyzed theoretically by Davis *et al.*, who studied the coupling between a plasmonic nanoparticle and a small dielectric sphere in the quasistatic limit [16, 17]. Here we present an alternative approach that results in a description of the LSPR shift in terms of changes in local field intensities due to the presence of the analyte. We begin by describing the analyzed system in terms of coupled point dipoles to provide a general background. Next, we describe a model based on the quasistatic approximation that is based on an analysis of local fields. It allows for estimation of the magnitude of the LSPR shift as a function of the location of the dielectric analyte and takes into account its material and geometrical size. As a test case, we assume that the metal resonator and analyte are both spherical in shape. Finally, we compare and discuss the analytical model in relation to Finite Difference Time Domain (FDTD) simulations of a gold nanorod and a nanodisk coupled to a small dielectric object.

## 2. Coupled dipole approximation

The interaction of two objects with dimensions smaller than the wavelength of the illuminating light may be analyzed within a coupled dipole approximation, which is a self-consistent solution to a problem of scattering electromagnetic fields by the system. The particles are assumed to be characterized only by an electric dipole polarization $P_i = \alpha_i(E_{i0} - \sum_{j\neq i} A_{ij}P_j)$ dependent on the local electric field coming from the source $E_{i0}$ and other dipoles $A_{ij}P_j$ and its polarizability $\alpha_i$. To make our point we drop all vector and matrix indices and look at the following set of equations for a dipole $P_1$ coupled to a dipole $P_2$:

$$P_1 = \alpha_1 \left(E_0 - A_{12}P_2\right), \tag{1a}$$

$$P_2 = \alpha_2 \left(E_0 - A_{21}P_1\right), \tag{1b}$$

where $E_0$ is the extarnal field strength (assumed to be the same for both dipoles) and $A_{12}$ is the dipole coupling factor. We are interested in the new mode frequencies of the second particle, assumed to be metallic, due to its interaction with the first being a dielectric. Substituting Eq. 1a into Eq. 1b we obtain the self-consistent polarizability of the metal object

$$P_2 = \frac{\alpha_2\left(1-\alpha_1 A_{21}\right)}{1-\alpha_1\alpha_2 A_{12}A_{21}}E_0. \tag{2}$$

Setting the denominator to zero: $1-\alpha_1\alpha_2 A_{12}A_{21} = 0$ allows us to calculate the mode frequencies of the interacting system. We assume that the polarizability $\alpha_i = 4\pi\varepsilon_0 r_i^3 \frac{\varepsilon_i - 1}{\varepsilon_i + 2}$, where $i = 1,2$, $r_i$ is the radius of sphere $i$ and $\varepsilon_0$ is the permittivity of free space. Solving for $\varepsilon_2(\omega)$ we obtain

$$\varepsilon_2(\omega) = -\frac{2+Q}{1-Q}, \tag{3}$$

where $Q \equiv (4\pi\varepsilon_0)^2 \left(r_1 r_2\right)^3 \frac{\varepsilon_1 - 1}{\varepsilon_1 + 2} A^2$ is a parameter that depends on the mutual couping of the two dipoles $(A_{12} = A_{21} = A)$, their radii and permittivity $\varepsilon_1$ of the dielectric. Let us assume that $\varepsilon_2$ is described by a Drude model: $\varepsilon_2 = 1-\omega_p^2/\omega^2 \equiv 1-\Omega^{-2}$, where $\omega_p$ is the plasma frequency. For a lone metal sphere (resonance frequency $\omega_0$) we have $\Omega_0^2 = \frac{1}{3}$, while at the shifted frequency $\omega_1$ it is $\Omega_1^2 = \Omega_0^2(1-Q)$. The normalized resonance shift due to the interaction is then equal to

$$\overline{\Delta\omega} \equiv \frac{\omega_1 - \omega_0}{\omega_0} \simeq \frac{\omega_1^2 - \omega_0^2}{2\omega_0^2} = \frac{1}{2}\left(\frac{\Omega_1^2}{\Omega_0^2} - 1\right) = -\frac{1}{2}Q. \tag{4}$$

We see that the resonance peak shift is directly proportional to the coupling strength $Q$. In the near-field we can use $A \sim 1/(4\pi\varepsilon_0 d^3)$, where $d$ is the distance between the dipoles. Thus, for a small analyte ($r_1$) placed on the surface of the metal sphere ($r_2$) we have $d \approx r_2 \gg r_1$

$$-\frac{1}{2}Q \sim -\frac{1}{2}\frac{V_1}{V_2}\frac{\varepsilon_1 - 1}{\varepsilon_1 + 2}. \tag{5}$$

From this simple analysis we see, that the expected resonance shift is proportional to the relative volumes of the analyte and resonator and depends on the polarizability of the analyte. If we take into account the fact that the dipole coupling terms determine the electric field acting onto the other dipole ($Q \sim A^2$), we see that the magnitude of the shift is proportional to the local electric field enhancement. Moreover, in the full case $A$ is a tensor, so the dipole orientation with respect to the external field also influences the observed shift. Comparing this schematic result to the one obtained by Davis *et al.* [16] we note the qualitative agreement when neglecting the field orientation: both models reproduce the volume scaling and the saturation for large $\varepsilon_1$. Next, we will describe a way of calculating the resonance shift based on the local field intensities in the constituents of the resonant system, which is not limited to spherical geometries.

## 3. Quasistatic model

Let us consider an arbitrarily shaped metallic object in a dielectric medium illuminated by a plane wave of frequency $\omega$. The extinction spectrum and resonance frequency $\omega_0$ depend on its size, shape, and material properties as well as those of the surrounding medium. Binding of an additional object of permittivity different from the surrounding medium to its surface changes the resonance conditions, what can be observed by a slight shift of the spectrum. In the quasistatic limit, letting $\vec{E}$ denote the induced field due to an external field $\vec{E}_0$ impinging on the system, we can let $\vec{E} = -\vec{\nabla}\Psi$. An induced local field generated by a metal resonator decays to zero at a surface $S$ far away from the particle [18]. We then have ($\vec{\nabla} \cdot \vec{D} = 0$):

$$0 = -\oint_S \left(\Psi^* \vec{D}\right) \cdot d\vec{S} = -\int_V \vec{\nabla} \cdot \left(\Psi^* \vec{D}\right) dV = \int_V \vec{E}^* \cdot \vec{D} dV = \sum_i \varepsilon_i \int_{V_i} |E_i|^2 dV \equiv \sum_i \varepsilon_i I_i, \tag{6}$$

where $V$ is a volume enclosed by $S$ and the sum is over the electric field in individual subvolumes $V_i$ defined by their respective permittivities $\varepsilon_i$. In our case they are the metal $m$, dielectric analyte $d$ and surrounding medium $s$. Without an analyte Eq. 6 becomes

$$\varepsilon_m(\omega) I_m + \varepsilon_s I_s = 0, \tag{7}$$

which determines the resonance frequency $\omega_0$. For a spherical particle $I_s = 2I_m$ and we retrieve the well-known condition $\varepsilon_m(\omega) + 2\varepsilon_s = 0$ for a surface plasmon resonance. When we add a dielectric object $d$, the resonance is shifted and broadened by $\Delta\omega$, and 7 is modified to

$$\varepsilon_m(\omega') I'_m + \varepsilon_s I'_{s'} + \varepsilon_d I_d = 0, \tag{8}$$

where $'$ indicates changes compared to Eq. 7. To determine the relative resonance shift $\overline{\Delta\omega} \equiv \frac{\omega' - \omega_0}{\omega_0}$, we expand the permittivity $\varepsilon_m(\omega')$ of the metal object into a Taylor series

$$\varepsilon_m(\omega') = \varepsilon_m(\omega_0) + \omega_0 \overline{\Delta\omega} \left.\frac{\partial \varepsilon_m}{\partial \omega}\right|_{\omega_0} + \ldots, \tag{9}$$

Subtracting Eq. 7 from Eq. 8 and substituting $\varepsilon_m(\omega')$ into the result we obtain

$$\overbrace{\varepsilon_m(\omega_0)\left(I'_m - I_m\right) + \omega_0 \overline{\Delta\omega} \left.\frac{\partial \varepsilon_m}{\partial \omega}\right|_{\omega_0} I'_m}^{\text{I. field change in metal object and change in resonance frequency}} + \overbrace{\varepsilon_d I_d + \varepsilon_s \left(I'_{s'} - I_s\right)}^{\text{II. field and volume change outside metal object}} = 0. \tag{10}$$

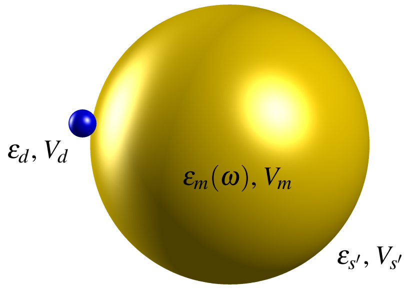

Fig. 1. Schematic view of a dielectric analyte ($\varepsilon_d$, $V_d$) attached to a metal sphere ($\varepsilon_m(\omega)$, $V_m$) surrounded by a dielectric medium ($\varepsilon_{s'}$, $V_{s'}$).

Equation 10 from which we can now calculate $\overline{\Delta\omega}$ consists of two parts. The first part (I) depends on the field change inside the metal resonator brought on by the analyte and the second (II) part depends on the volume and field change in the surrounding medium.

We rewrite Eq. 10 into a form that allows for an explicit estimation of the resonance frequency shift from the electric fields which may be obtained using different methods. The dielectric particle decreases the outside volume by $V_d$ giving a new surrounding medium volume $V_{s'} = V_s - V_d$ and we can split the secong term of II into two parts. Additionally, we assume, that the analyte is small compared to the resonator ($V_d \ll V_m$), so that the perturbed field in the resonator is approximated by the field of the unperturbed one $I'_m \approx I_m$, however, this approximation is used only in the second term of Eq. 10. Rearranging Eq. 10 we then obtain a formula for the relative frequency shift

$$\overline{\Delta\omega} = -\frac{\sum_i (\varepsilon_i I_i - \varepsilon_i^0 I_i^0)}{\omega_0 \left.\frac{\partial \varepsilon_m}{\partial \omega}\right|_{\omega_0} I_m}, \tag{11}$$

where the shift is proportional to a sum over spatial integrations of fields in individual subvolumes $i$ and $I_i^0$ indicates unperturbed (no analyte) fields. Notice that this is a general result, whereby the shift is related to the change in stored electromagnetic energy in the system as the analyte is introduced. The real part $\Re\{\}$ of $\overline{\Delta\omega}$ gives the shift and its imaginary part $\Im\{\}$ the change in width of the large particle resonance.

We will now apply this formula to a simple test case of a gold sphere (radius $r_m = 30$ nm) with a spherical analyte ($r_d = 1$ nm) limiting the number to three components $m$, $s$, and $d$ (see Fig. 1). The considered gold sphere has maximum extinction at 585 THz and at this frequency permittivity $\varepsilon_m = -3.21 + 2.91\mathrm{i}$ and its derivative $\omega_0 \frac{\partial \varepsilon_m}{\partial \omega}\big|_{\omega_0} = 30.18 + 22.51\mathrm{i}$. These values are calculated from experimental data of Johnson and Christy [19].

In Fig. 2 we plot cross-sections of spatial distributions the numerator of Eq. 11 showing the magnitude and sign of the contributions for a parallel ($\beta = 0$) and perpendicular ($\beta = \pi/2$) field alignment in Fig. 2a and b, respectively. When $\beta = 0$ the analyte is located at the incident side of the metal sphere on the $z$-axis, while $\beta = \pi/2$ means that the analyte is on the side where the resonant field is the strongest. The energy redistribution due to analyte adhesion in the considered case is the following: the difference of the product of the permittivity and the integral between the perturbed and unperturbed fields in the metal gives a negative contribution to the total shift, while in the surrounding medium it has a positive sign. In the dielectric particle the sign depends on the permittivity of the analyte – in the case presented for $\varepsilon_d = 4$ the contribution is positive.

To obtain these cross-sections as well as resonance shift plots in Fig. 2 we take into account that the analyte is much smaller than the resonator and that the local radius of curva-

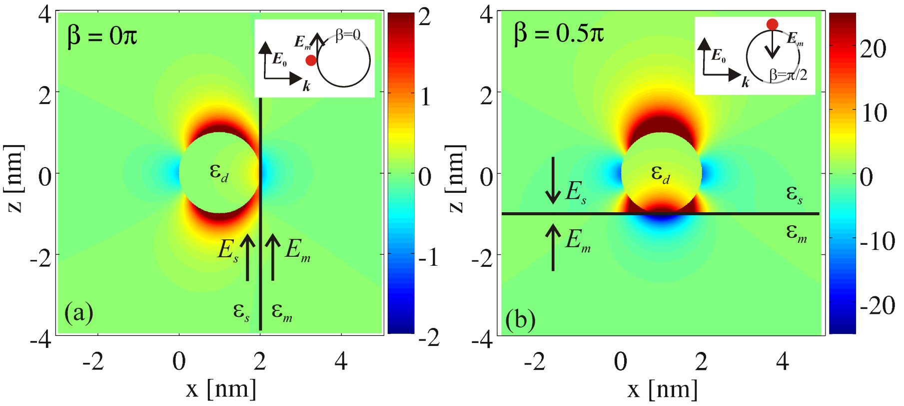

Fig. 2. Local values of the sum of integrals in the numerator of Eq. 11 calculated for a dielectric analyte of $\varepsilon_d = 4$, $r_d = 1$ nm attached to a gold resonator ($\varepsilon_m = -3.21 + 2.91\mathrm{i}$, $r_m = 30$ nm) in vacuum ($\varepsilon_s = 1$) for the local electric field in metal $E_m$ (a) parallel and (b) perpendicular to the surface. The contribution from the metal is negative and causes a blueshift. The contributions from the surrounding medium and the analyte for $\varepsilon_d = 4$ are positive and cause a redshift. The insets in (a) and (b) show the system scheme for $\beta = 0$ and $\beta = \pi/2$, respectively, where the dielectric particle is a red circle on the metal resonator placed in an incident field $E_0$..

ture of the resonator is larger than the dielectric particle size. For a sphere the image factor is $(\varepsilon_m - \varepsilon_s)/(\varepsilon_m + \frac{l+1}{l}\varepsilon_s)$ and its response at close distances is determined by large $l$, which then approaches the planar image factor $(\varepsilon_m - \varepsilon_s)/(\varepsilon_m + \varepsilon_s)$. This allows us to locally model the gold surface as flat. The analyte is placed in the near-field of the metal resonator and its dipolar response is determined by its polarizability $\alpha_d \propto (\varepsilon_d - \varepsilon_s)/(\varepsilon_d + 2\varepsilon_s)$. The induced dipole, decomposed into parallel and perpendicular components relative to the local metal surface, changes the local electric field which we calculate in the quasistatic case using the method of images. The change to the field outside the resonator is generated by the original dipole and a mirrored one inside the metal, the change inside the metal by the original and an image outside, and inside the dielectric particle by the image in the metal and the presence of the particle itself.

## 4. Results and discussion

Figure 3a shows the calculated resonance shift $\Re\{\overline{\Delta\omega}\}$ as a function of the analyte permittivity $\varepsilon_d$ and the angle $\beta$ with black points. The shift is a monotonic function of permittivity, because for an increasing $\varepsilon_d$ the dipole moment increases asymptotically due to saturation of the dielectric sphere polarizability (full saturation is not shown here). Figure 3b and c show the total shift predicted by the model $\overline{\Delta\omega}$ (solid blue line) and calculated with FDTD $\overline{\Delta\omega}_{\mathrm{FDTD}}$ (dashed black line with circles), and individual contributions from the three subvolumes ($\overline{\Delta\omega} = \overline{\Delta\omega}_{s'} + \overline{\Delta\omega}_m + \overline{\Delta\omega}_d$) for $\beta = 0$ and $\pi/2$, respectively. We notice, that the model agrees quite well with the full FDTD calculation, although the latter is a fully-retarded method and takes into account the radiative components. For small $\varepsilon_d$ the main redshift comes from the surrounding medium $\overline{\Delta\omega}_{s'}$ and analyte $\overline{\Delta\omega}_d$ and is reduced by the remaining volume. For large $\varepsilon_d$ the analyte volume also decreases the redshift. When the field is perpendicular to the surface instead of parallel, the electric field amplitude, determined by $\beta$, increases giving a larger shift.

The angular dependence is, in a first approximation, of the form $\cos^2\beta + b|\frac{\varepsilon_m}{\varepsilon_s}|^2\sin^2\beta$, where $b$ is a parameter determining the relative sensitivity to the presence of an analyte placed in a parallel or perpendicular electric field with respect to the surface. If the shift is only propor-

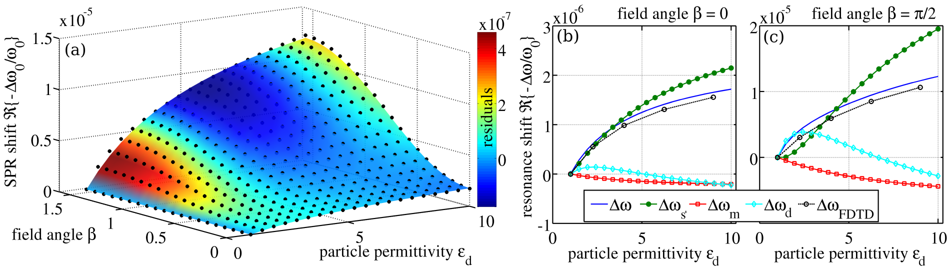

Fig. 3. (a) Resonance shift $\Re\left\{\overline{\Delta\omega}\right\}$ as function of $\varepsilon_d$ and $\beta$ for an analyte of $r_d = 1$ nm attached to a gold resonator $r_m = 30$ nm in vacuum ($\varepsilon_s = 1$): black points – calculated with model, surface – Eq. 12 fitted to data, color scale for surface – residuals. (b)-(c) Total resonance shift $\Re\{\overline{\Delta\omega} = \sum_{i=m,d,s'} \overline{\Delta\omega_i}\}$, contributions from subvolumes $\Re\left\{\overline{\Delta\omega}_{i=m,d,s'}\right\}$, and shift obtained with FDTD $\overline{\Delta\omega_{\mathrm{FDTD}}}$ for (b) a parallel ($\beta = 0$) and (c) perpendicular ($\beta = \pi/2$) field. Notice the different scales for $\beta = 0$ and $\beta = \pi/2$

tional to the intensity of the local field $|E|^2$ determined by the position of the analyte, and by the permittivity of gold at the resonance frequency $\omega_0$, then $b = 1$ . To estimate $b$ we fit the following function

$$a_0 \frac{\varepsilon_d - 1}{\varepsilon_d + a_1} \left( \cos^2 \beta + b_0 \left| \frac{\varepsilon_m}{\varepsilon_s} \right|^2 \sin^2 \beta \right), \qquad (12)$$

to the calculated data points. The result of the fitting ($a_0 = 2.71 \times 10^{-6}$, $a_1 = 3.98$, and $b_0 = 0.37$), as can be seen in Fig. 3a, is presented using a 3D-surface, while the surface's color scale shows the residuals of the fit. From the fitting procedure we get $b_0 \approx 0.37$, which means that the sensitivity per field unit is larger for the field along the metal surface than perpendicular to it. This is also confirmed in our FDTD simulations.

Within the assumed model the frequency shift is proportional to the normalized volume $V_d/V_m$ of the dielectric analyte and is confirmed in Fig. 4, where the largest considered normalized analyte volume corresponds to a radius of 2 nm. The field decays away from the gold sphere, so the resonance shift increases more slowly than a linear function and will approach asymptotically a maximum value in a similar manner as observed for gold nanoislands [20]. However, this last observation is beyond this quasistatic approximation as the analyte size would have to be comparable in size to the metal sphere.

To see how the method performs for commonly encounted sensors, we check how it com-

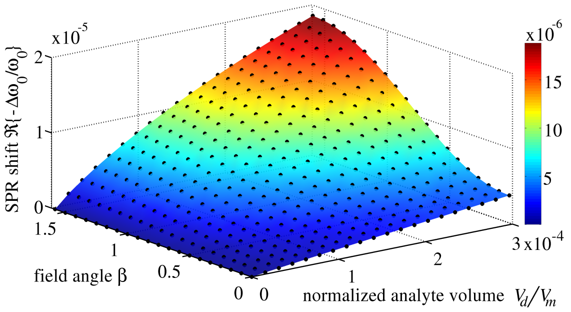

Fig. 4. Resonance shift $\Re\left\{\overline{\Delta\omega}\right\}$ as function of normalized particle volume $V_d/V_m$ and angle $\beta$ calculated for a dielectric particle with $\varepsilon_d = 2$.

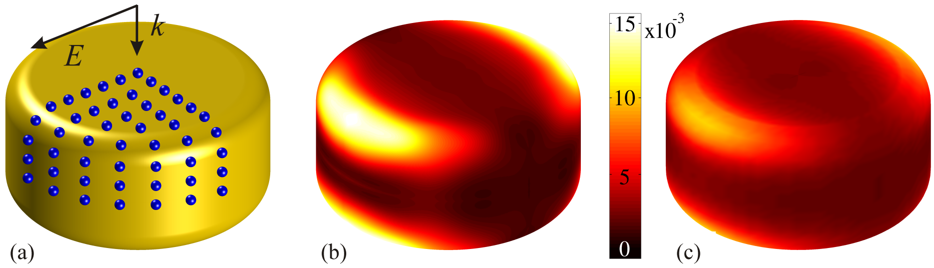

Fig. 5. (a) Gold disk of radius 25 nm, thickness 25 nm, edge curvature 5 nm illuminated by a plane wave. Blue spheres indicate positions of analyte placement for FDTD calculations. (b) Resonance shift calculated using FDTD at positions from (a) and interpolated using cubic splines for easier comparison with model calcuated shift. (c) Resonance shift calculated with the model. The color scale is the same for (b) and (c).

pares with FDTD simulations for predicting resonance shifts for a disk-shaped resonator (Fig. 5a) with the following dimensions: radius 25 nm, thickness 25 nm, edge curvature 5 nm, which is illuminated by a linearly polarized plane wave. The analyte is modeled as a dielectric sphere with permittivity $\varepsilon_d = 4$ and radius of $r_d = 1$ nm and is arranged sequentially in a lattice on the surface of the disk. We calculate the extinction spectra using 3D-FDTD with nonuniform meshing equal to 0.5 nm for the gold disk and 0.2 nm for the dielectric analyte. Resonance shifts, shown in Fig. 5b, are obtained by fitting the data points and extracting the local maximum of the fitted function. Resonance shift values between the particle placements are obtained by interpolating with cubic splines. For the disk, the accuarcy of the fit does not depend on the location of the analyte and is $\pm 0.2 \times 10^{-3}$ nm. The electric field distribution for the model is calculated at resonance (534.7 nm) of a lone disk and is used, in a similar scheme as discussed for the sphere, to estimate the peak shifts (Fig. 5c). We see, that the agreement is very good when the analyte is placed far away from the edges of the disk, however, decreases when moving away from the center. The largest mismatch is observed when the analyte is placed in the vicinity of the curved edge - the FDTD simulation yields a $1.5 \times 10^{-2}$ nm shift, while using the model we estimate a $1.0 \times 10^{-2}$. The reason behind this is the calculation scheme for the dipole moments of the analyte and its image – we assume a much larger local curvature of the surface of the metal resonator than the analyte. This condition is not fulfilled when the dielectric particle is near the rounded edge. However, a method of calculating electromagnetic fields created by an electric dipole in the vicinity of a sphere in the quasistatic approximation, presented by Zurita-Sánchez [21], may be modified to correct the model prediction.

A second comparison of model predicted shifts to FDTD obtained ones is carried out for a gold rod (radius of caps and rod 20 nm, length 100 nm) with dielectric particles ($r_d = 1$ nm, $\varepsilon_d = 4$) arranged at 13 positions along a line as indicated in Fig. 6. The longitudinal dimension of the rod relative to the resonance wavelength is about four times larger so the quasistatic condition is not fulfilled as strongly as in the previous case. Thus, there is a larger discrepancy of the quantitative results obtained via FDTD (simulations and extinction fitting) and model calculated data. The shifts are schematically indicated by lines following the surface of the rod where the analyte molecules are placed: the blue solid line represents fits to FDTD obtained shifts (maximum resonance shift is $3.7 \times 10^{-3}$ nm, $\overline{\Delta\omega} = 7.4 \times 10^{-6}$) with a 95% confidence interval shown using the green dashed line; the solid red line indicates model calculated shifts. Quantitative matching is not as good as in the test case of a sphere, but due to a larger radius of curvature of the resonator is better than for analytes near the disk edge.

Our approach of calculating the plasmon resonance shift of a metallic resonator due to dielec-

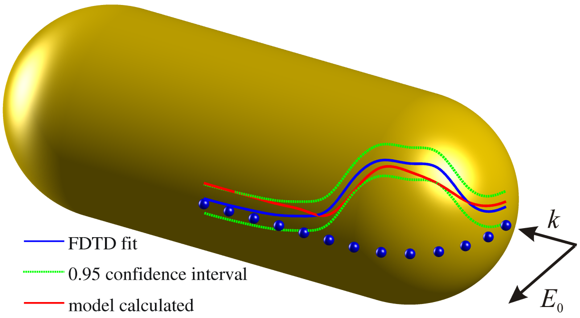

Fig. 6. Gold rod 20 nm in radius with hemispherical caps of 100 nm long with schematically indicated positions of analyte placement illuminated with a plane wave polarized along the *x* axis. The analytes are placed along a line parallel to the incident electric field as indicated by blue spheres. FDTD calculated/fitted resonance shifts are indicated by the blue line with 0.95 confidence interval (green dashed). The shift calculated using the model is shown by the red line.

tric particle adhesion can be viewed in light of dipole – image-dipole interaction. An electric field parallel to the surface induces a parallel dipole moment in the analyte, while its image is antiparallel. For the electric field perpendicular to the surface, both the dipole and its image have the same sense. Both arrangements form an attractive system leading to a lower resonance frequency, but, in the case of the perpendicular field the interaction is weaker and for an outside field of the same amplitude as for a parallel field produces a smaller shift. However, the larger field enhancement counteracts this.

## 5. Conclusions

We have demonstrated a method of estimating the resonance shift of a simple metal object due to adhesion of a small dielectric analyte within the quasistatic approximation. It requires only a single, prior calculation of electromagnetic fields surrounding the resonator without the analyte using a numerical method, while its accuracy depends on the estimation quality of the analyte polarizability. Using FDTD simulations and the quasistatic model we have demonstrated the dependence of the plasmon resonance of metallic objects on the location of the added dielectric analyte. The magnitude of the shift is a function of geometrical and material parameters as well as position and is consistent with a schematic coupled dipole picture. The sensitivity per electric field unit in which the analyte is placed is greater when the field is parallel to the metal surface than for perpendicular alignment. However, due to a large enhancement factor observed for the latter arrangement shifts in this configurations are greater.

## Acknowledgements

We acknowledge support from the Swedish Foundation for Strategic Research via the Functional Electromagnetic Metamaterials project SSF RMA08.